Effect of B on the Microstructure and Mechanical Properties of Mechanically Milled TiAl Alloys

SANG H. KIM, H.H. CHUNG, SUNG G. PYO, S.J. HWANG, and NACK J. KIM

The present study is concerned with γ-$(Ti_{52}Al_{48})_{100-x}B_x$ (x = 0, 0.5, 2, 5) alloys produced by mechanical milling/vacuum hot pressing (VHPing) using melt-extracted powders. Microstructure of the as–vacuum hot pressed (VHPed) alloys exhibits a duplex equiaxed microstructure of α_2 and γ with a mean grain size of 200 nm. Besides α_2 and γ phases, binary and 0.5 pct B alloys contain Ti_2AlN and Al_2O_3 phases located along the grain boundaries and show appreciable coarsening in grain and dispersoid sizes during annealing treatment at 1300 °C for 5 hours. On the other hand, 2 pct B and 5 pct B alloys contain fine boride particles within the γ grains and show minimal coarsening during annealing. Room-temperature compressing tests of the as-VHPed alloys show low ductility, but very high yield strength > 2100 MPa. After annealing treatment, mechanically milled alloys show much higher yield strength than conventional powder metallurgy and ingot metallurgy processed alloys, with equivalent ductility to ingot metallurgy processed alloys. The 5 pct B alloy with the smallest grain size shows higher yield strength than binary alloy up to the test temperature of 700 °C. At 850 °C, 5 pct B alloy shows much lower strength than the binary alloy, indicating that the deformation of fine 5 pct B alloy is dominated by the grain boundary sliding mechanism.

I. INTRODUCTION

INTERMETALLIC compounds based on TiAl are being recognized as potential high-temperature structural materials because of their excellent oxidation resistance, high thermal conductivity, and low density.[1–5] However, their general lack of ambient temperature ductility and high-temperature creep resistance has led to a number of alloy design paths being pursued for improvement of their properties. One of the processing paths that has shown potential for enhancing ductility and fracture toughness is mechanical milling/alloying.[5–8] This technique produces powders with a fine nanoscale grain size and a homogeneous distribution of dispersoids. However, it is often found that the nanoscale microstructure of mechanically milled/alloyed powders is lost during consolidation. Oxide or nitride dispersoids formed during mechanical milling/alloying are quite effective in retarding grain growth in some cases; however, this is not the case for the alloys such as NiAl or TiAl, which require high-temperature consolidation and heat treatment.[9] Although mechanically milled/alloyed alloys still show much finer grain size after consolidation than conventionally processed alloys, it is needed to restrict grain growth as much as possible to maximize the potential of mechanically milled/alloyed alloys.

The present study is aimed at investigating the microstructure and mechanical properties of mechanically milled TiAl alloys alloyed with B. It has been shown that TiB_2 phase formed by adding B to TiAl alloys has a significant effect on grain refinement in ingot cast alloys.[10] It has also been shown that TiB_2 is very thermally stable, rarely reacting with the matrix even at the high temperature of 1200 °C.[11] Accordingly, taking advantage of the dispersion of TiB_2 phase, attempts have been made to improve the fracture toughness, creep strength, high-temperature formability, *etc.* of ingot-cast TiAl alloys.[12,13] It is thought that the mechanical milling process is more effective in utilizing the beneficial effect of dispersoids than the ingot cast process, since the former can distribute dispersoids more uniformly in the matrix.

II. EXPERIMENTAL PROCEDURE

Alloy powders of $Ti_{52}Al_{48}$ and $(Ti_{52}Al_{48})_{100-x}$ B_x (x = 0.5, 2, 5) compositions were made by the melt extraction method. These powders were mechanically milled for 100 hours in the attritor mill under Ar atmosphere with the weight ratio of ball to powder of 20:1. Details of experimental procedures for melt extraction and mechanical milling can be found elsewhere.[14] These mechanically milled powders were consolidated by vacuum hot pressing (VHPing) at 1000 °C for 2 hours under 87 MPa load. After consolidation, billets were annealed for 5 hours at 1300 °C, followed by either air cooling of furnace cooling. To evaluate the mechanical properties, compression tests were conducted on electro-discharge machining processed specimens (3 mm in diameter and 6 mm long) at the constant strain rate of 3.45×10^{-4}/s and at the temperatures ranging from room temperature to 850 °C. No lubricant was used for compression test. Strain rate sensitivity (m) values were

SANG H. KIM, Graduate Student, and NACK J. KIM, Professor, are with the Center for Advanced Aerospace Materials and Department of Materials Science and Engineering, Pohang University of Science and Technology, Pohang 790-784, Korea. H.H. CHUNG, Senior Researcher, is with the R & D Center, Korea Gas Corporation, Kyunggi 425-150, Korea. SUNG G. PYO, Senior Researcher, is with Hyundai Electronics Industries Co., Ltd., Kyunggi 467-701, Korea. S.J. HWANG, Assistant Professor, is with the Department of Materials Engineering, Daejin University, Kyunggi 487-711, Korea.

This article is based on a presentation made in the symposium ''Mechanical Behavior of Bulk Nanocrystalline Solids,'' presented at the 1997 Fall TMS Meeting and Materials Week, September 14–18, 1997, in Indianapolis, Indiana, under the auspices of the Mechanical Metallurgy (SMD), Powder Materials (MDMD), and Chemistry and Physics of Materials (EMPMD/SMD) Committees.

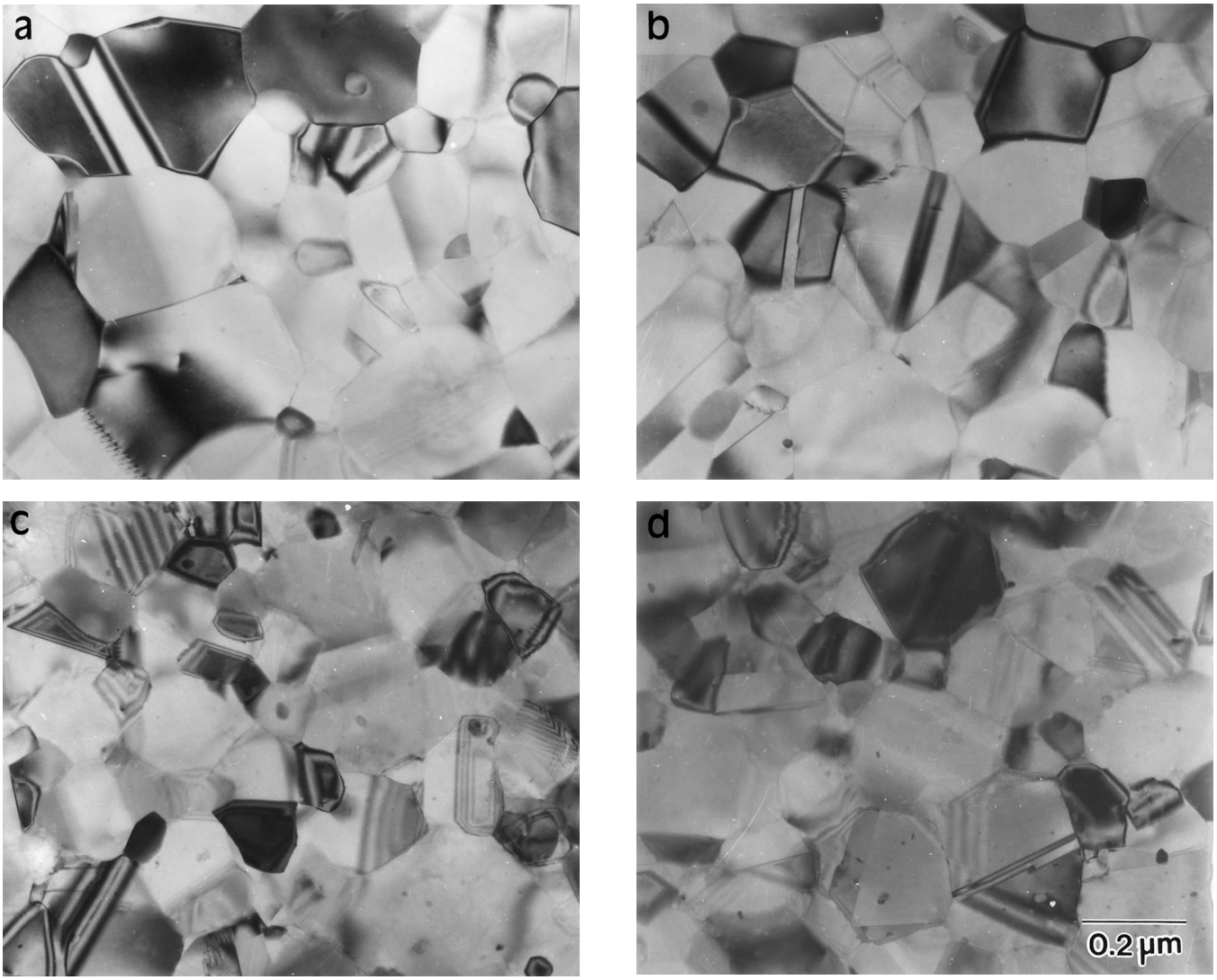

Fig. 1—Bright-field TEM micrographs of mechanically milled TiAl alloys after VHPing: (*a*) 0 pct B, (*b*) 0.5 pct B, (*c*) 2 pct B, and (*d*) 5 pct B.

Table I. Grain Size (μm) of Various Mechanically Milled Alloys

	0 Pct B	0.5 Pct B	2 Pct B	5 Pct B
As-VHPed	0.205	0.183	0.180	0.182
Annealed (AC)*	1.393	1.368	0.507	0.411
Annealed (FC)*	1.404	1.375	0.549	0.506

*AC and FC: air-cooled and furnace-cooled after annealing at 1300 °C for 5 h.

calculated from the variations of flow stress at the strain rates of 1.5×10^{-4}/s, 3.45×10^{-4}/s, and 1×10^{-3}/s and at 850 °C. To find out the effect of mechanical milling process, compression tests were also conducted on the vacuum hot pressed (VHPed) billets consolidated with melt-extracted powders. Microstructure of specimens was analyzed by X-ray diffraction (XRD) and analytical electron microscopy. Transmission electron microscopy (TEM) specimens were jet-polished at −35 °C using a solution of methanol 600 mL, *n*-butylalchol 350 mL, and perchloric acid 50 mL.

III. RESULTS AND DISCUSSION

A. *Microstructure*

Microstructure of the as-VHPed specimens (Figure 1) exhibits an equiaxed grain structure with a mean grain size of about 180 to 205 nm. It is seem that B has no appreciable effect on the grain size of as-VHPed specimens (Table 1). The XRD analysis of these as-VHPed specimens indicates that their microstructures basically consist of γ-TiAl and a small amount of α_2 phase (Figure 2). In the case of 0 pct B and 0.5 pct B alloys, Ti_2AlN and α-Al_2O_3 phases are present in a small amount, while in 2 pct B and 5 pct B alloys, TiB_2 and TiB phases are present with a negligible amount of Ti_2AlN phase and no α-Al_2O_3 phase. Closer examination of the microstructures of 0 pct B (Figure 1(a)) and 0.5 pct B (Figure 1(b)) alloys reveals that Ti_2AlN and α-Al_2O_3 phases sized 30 to 50 nm are located along the γ grain boundaries without any dispersoids present inside the grains. The α_2-Ti_3Al phase is present as discrete particles along the γ grain boundaries as opposed to the thin lamellae found in ingot cast alloys. Microstructure of as-VHPed alloys can be characterized as duplex equiaxed grain struc-

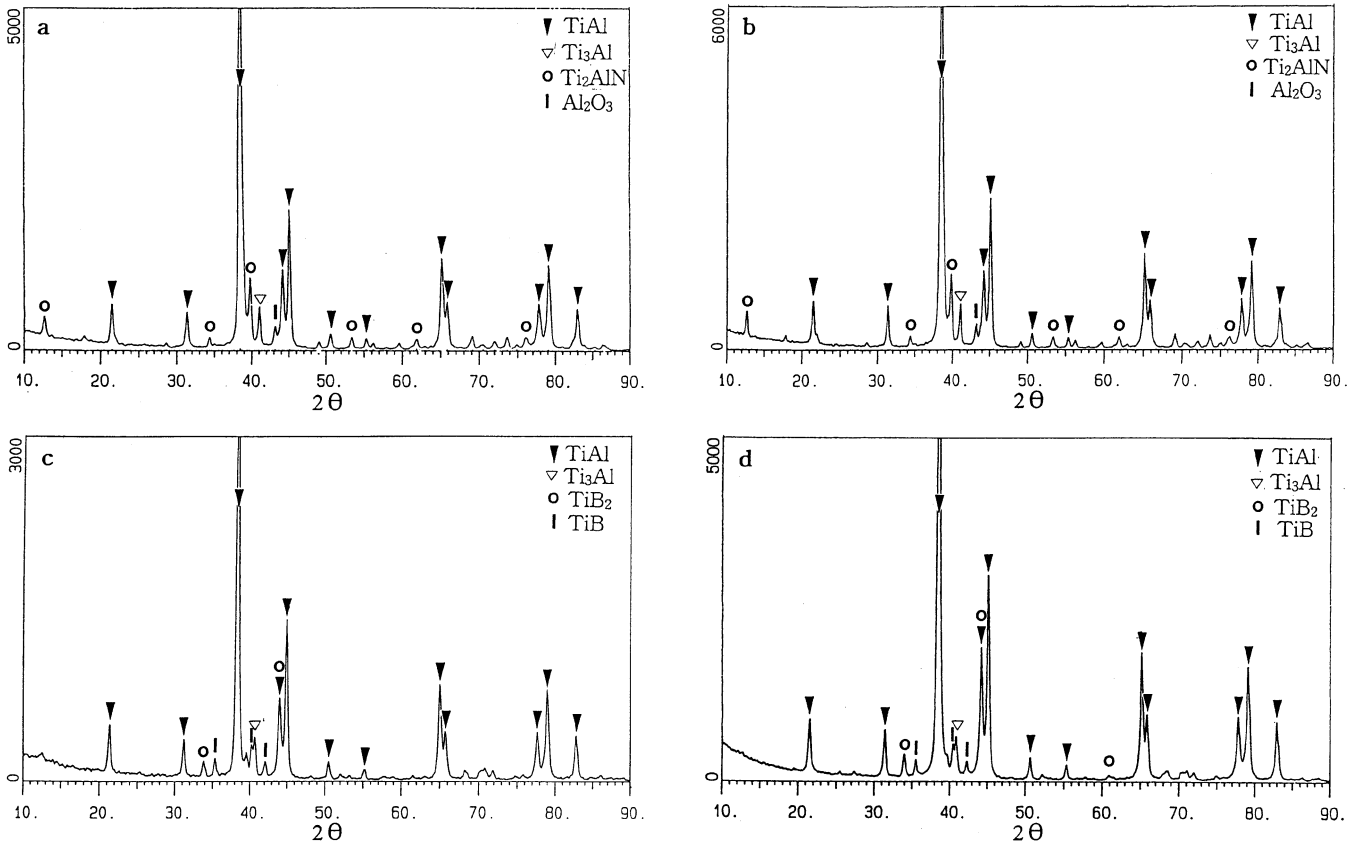

Fig. 2—XRD patterns of mechanically milled TiAl alloys after VHPing: (*a*) 0 pct B, (*b*) 0.5 pct B, (*c*) 2 pct B, and (*d*) 5 pct B.

ture.[15,16] It is known that lamellar grains are generally formed when TiAl alloy with ($\alpha_2 + \gamma$) two-phase composition is exposed to the high-temperature α phase region, followed by slow cooling.[17,18] In the present study, the VHPing was conducted at 1000 °C, corresponding to the ($\alpha_2 + \gamma$) phase region. Accordingly, a duplex equiaxed grain structure resulted with no specific orientation relationship between α_2 and γ phases. In 0.5 pct B alloy, borides were not detected either by XRD analysis or TEM analysis. Based on this, it is thought that B is most likely in γ solid solution for 0.5 pct B alloy. On the other hand, microstructures of 2 pct B (Figure 1(c)) and 5 pct B (Figure 1(d)) alloys show the presence of very fine boride dispersoids (<10 nm) distributed within the γ grains.

Microstructure of the specimen annealed for 5 hours at 1300 °C followed by air cooling (Figure 3) has much coarser grains as compared to those of the as-VHPed specimens. The degree of coarsening varies considerably with the content of B, showing an increased resistance to coarsening as the B content increases (Table 1). The annealed microstructure also shows a duplex equiaxed grain structure in which α_2 phase is present as particles, similar to the as-VHPed microstructure. The thermomechanical treatment conditions that produce this duplex equiaxed grain structure are similar to those reported by Koeppe *et al.*[19] and Lombard *et al.*[20] Although the initial microstructure of their alloys was near lamellar, unlike in this experiment, the duplex equiaxed grain structure was obtained by heat treatment at 1200 °C to 1300 °C, corresponding to the ($\alpha + \gamma$) phase region after partially spheroidizing the initial lamella structure by hot-working processes at 1050 °C or 1025 °C corresponding to the ($\alpha_2 + \gamma$) phase region. Such thermomechanical treatment conditions are quite similar to those used in the present study (VHPing at 1000 °C and heat treatment at 1300 °C). Coarse lamellar grains are formed when the heat-treatment temperature is within the α phase region.[20] It is known that the α_2 phase in such duplex equiaxed grain structure suppresses the coarsening of γ phase during heat treatment in the ($\alpha + \gamma$) phase region, thus stabilizing the microstructure even after being exposed to high temperature.[21] In the present experiment, however, microstructure of 0 pct B alloy is not stable after 5 hours of exposure at 1300 °C, despite the presence of α_2, Al_2O_3, and Ti_2AlN phases. The growth of γ grains after high-temperature exposure is more effectively hindered by finer boride dispersoids, as shown in Figure 4, resulting in much finer microstructures for the B containing alloys than 0 pct B alloy. The microstructural analysis of 0 pct B alloy (Figure 5) exhibits that the α_2 phase and Ti_2AlN phase are distributed along the γ phase grain boundaries, Ti_2AlN having the following orientation relationship with the γ phase matrix:

$$[101]_\gamma // [11\bar{2}0]_{Ti2AlN},\ (\bar{1}\bar{1}1)_\gamma // (0001)_{Ti2AlN}$$

The Ti_2AlN phase is not detected by XRD analysis of the melt-extracted ribbon and the mechanically milled powders, but is shown after VHPing at 1000 °C. The presence of the Ti_2AlN phase indicates that N, which is supersaturated in γ solid solution during mechanical milling, reacts with Ti and Al during VHPing to form precipitates with the orientation relationship shown previously. This Ti_2AlN phase can also form during the mechanical milling process

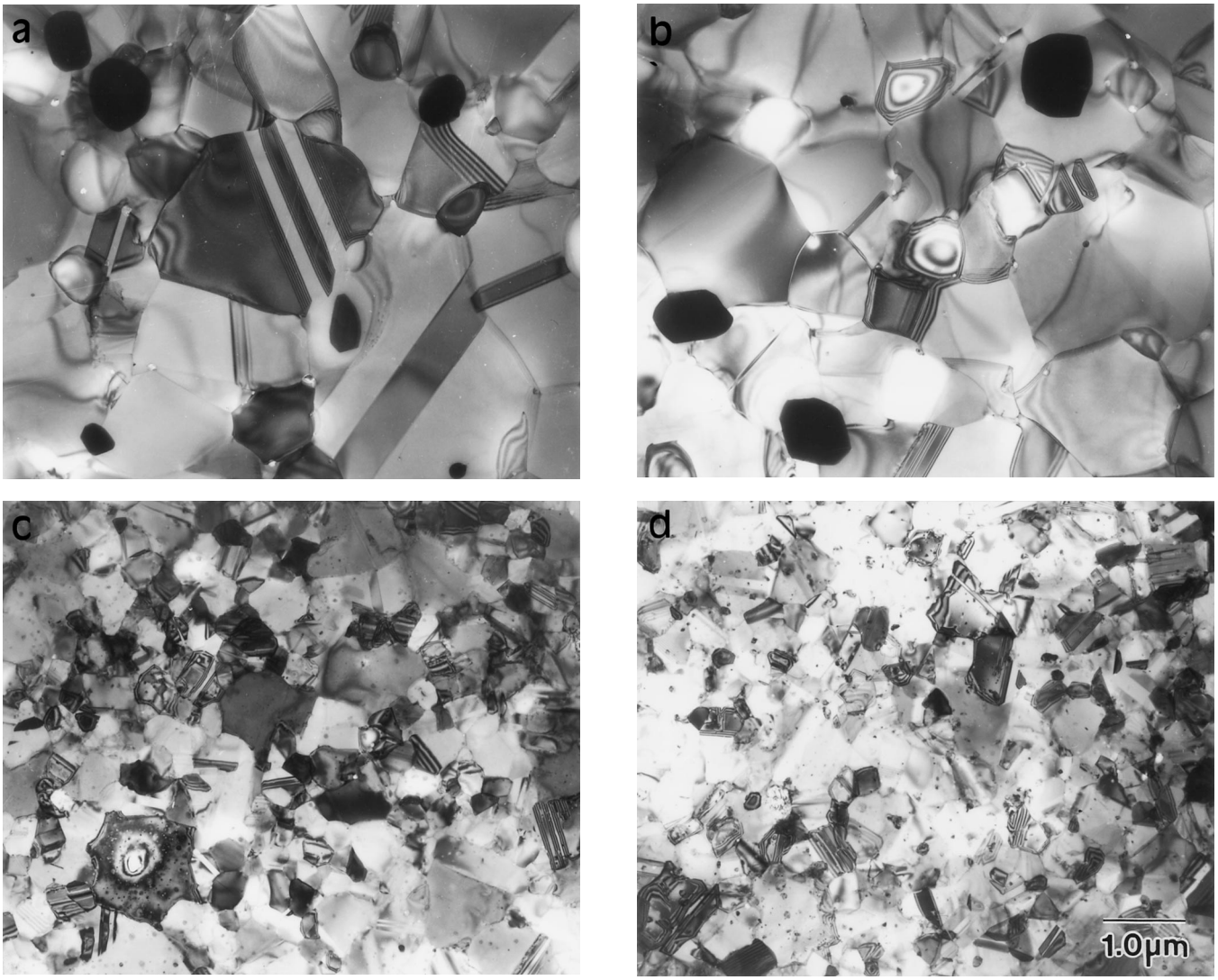

Fig. 3—Bright-field TEM micrographs of mechanically milled TiAl alloys after VHPing and annealing at 1300 °C for 5 h, followed by air cooling: (*a*) 0 pct B, (*b*) 0.5 pct B, (*c*) 2 pct B, and (*d*) 5 pct B.

of elemental Ti and Al powders under N_2 atmosphere.[22] It has been reported that Ti_2AlN forms at the time of combustion reaction of elemental Ti and Al powders under N_2 atmosphere, improving the high-temperature strength.[23] In the microstructure of 5 pct B alloy (Figure 4), it is observed that fine boride particles are dispersed inside the γ grains, together with the coarse TiB_2 particles. These fine boride dispersoids consist of TiB_2 and TiB phases according to selected area diffraction (SAD) pattern analysis. The TiB phase is not detected in XRD patterns of the melt-extracted ribbon and the mechanically milled powders, but is shown in the as-VHPed specimens. It is thought that TiB phase precipitates from γ-TiAl phase during VHPing at 1000 °C. Based on their study of the rapidly solidified Ti-(Al)-B alloys, Schwartz *et al.*[24] reported that TiB phase is formed in Ti-6B and Ti-25Al-4B alloys, while TiB_2 phase is formed in Ti-48Al-5B alloys. Hyman *et al.*[25,26] also reported that TiB is formed in a binary Ti-B alloy, while TiB_2 is formed in Ti-(48-50)Al-B alloys. They further showed that the morphology of boride changes with the content of B and the cooling rate and that TiB_2 can precipitate either from the supersaturated γ matrix *via* solid-state reaction or in the melt in blocky shape. In the present experiment, only TiB_2 is present in the melt-extracted TiAl-B alloy, similar to others' observations (Figure 6(a)). However, it is interesting to note that TiB phase precipitates from γ matrix during VHPing of mechanically milled powders at 1000 °C (Figure (6b)). According to Valencia *et al.*,[27] by adding Nb or Ta to Ti-(48-50)Al alloys having a similar composition to that used in this study, the TiB/TiB_2 phase boundary of ternary Ti-Al-B is moved in the direction toward the higher Al content, resulting in the formation of TiB phase instead of TiB_2 phase expected from the binary phase diagram. This indicates that the type of boride can be modified by the addition of tertiary elements as well as by the ratio of Ti and Al. The present study shows that only TiB_2 phase is present in the melt-extracted alloys, while TiB phase is also present in the mechanically milled alloys along with TiB_2 phase. It can be inferred that TiB phase is formed by accumulation of O and N during the mechanical milling process. Table II shows the contents of O and N and the type of borides observed in each processing stage. This sug-

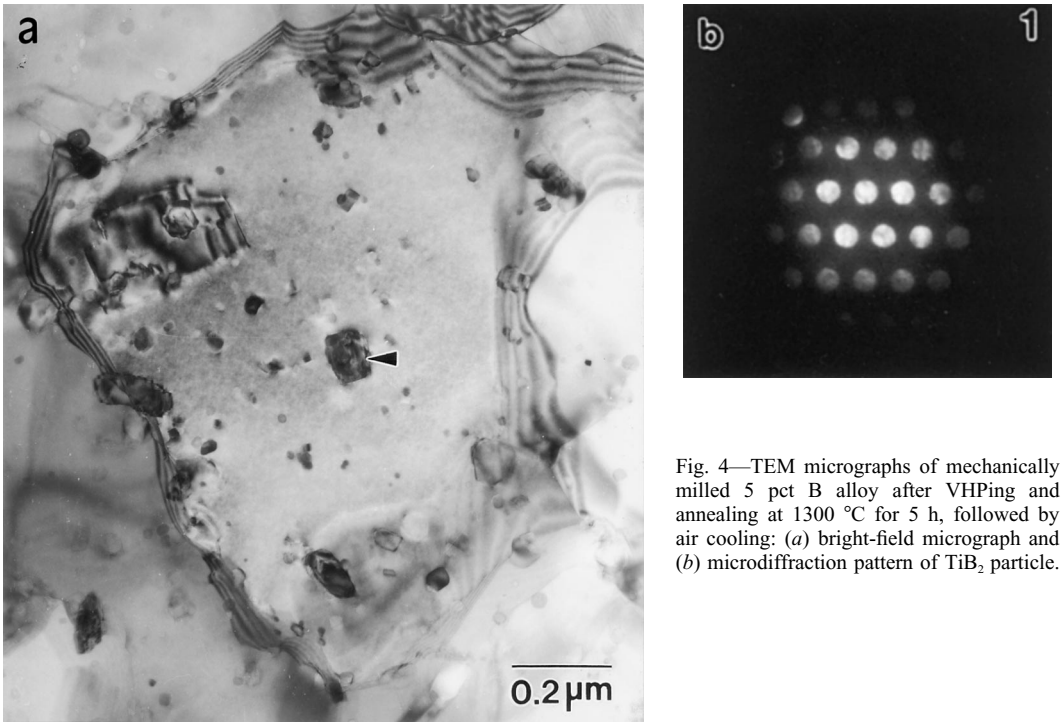

Fig. 4—TEM micrographs of mechanically milled 5 pct B alloy after VHPing and annealing at 1300 °C for 5 h, followed by air cooling: (*a*) bright-field micrograph and (*b*) microdiffraction pattern of TiB_2 particle.

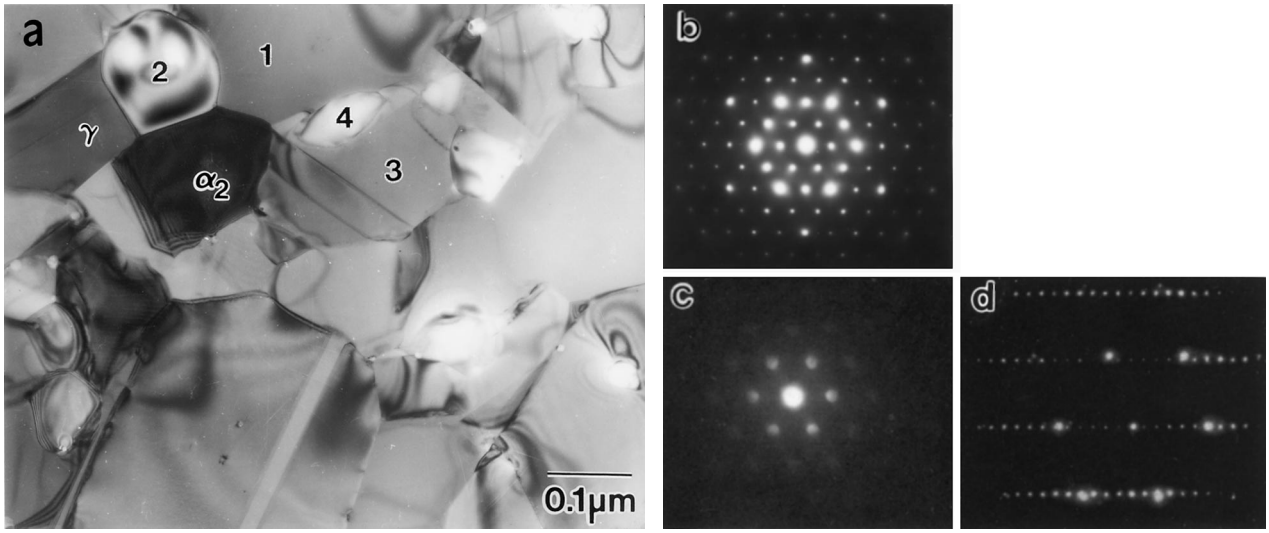

Fig. 5—TEM micrographs of mechanically milled 0 pct B alloy after VHPing and annealing at 1300 °C for 5 h, followed by air cooling: (*a*) bright-field micrograph, (*b*) SAD pattern of α_2-Ti_3Al phase (area 1) with $[0001]_{\alpha 2}$ zone axis, (*c*) SAD pattern of Ti_2AlN phase (area 2) with $[0001]_{Ti2AlN}$ zone axis, and (*d*) SAD pattern obtained from the Ti_2AlN and γ-TiAl phases (area 3 + 4) with $[101]_{\gamma}$ and $[1120]_{Ti2AlN}$ zone axes.

gests that O and N accumulated during the mechanical milling process shift the TiB/TiB_2 phase field, resulting in the formation of TiB phase.

Using XRD, the volume fraction of each phase can be calculated from the ratio of the peak heights of γ and α_2 phases.[28] Comparing the microstructure of the furnace-cooled with that of the air-cooled specimens shows that the volume fraction of α_2 in the furnace-cooled specimens is lower than that in the air-cooled specimens (Table III). It is well known that the reaction rate of γ precipitation from α by eutectoid transformation is far slower than that of ordering of α to α_2.[29] In fact, the γ precipitation can be suppressed by fast cooling, whereas the ordering to α_2 cannot be suppressed. Therefore, the air-cooled specimens have a higher α_2 volume fraction than the furnace-cooled specimens, since the transformation of α phase to γ is retarded as the cooling rate increases.

In the present study, there is a significant coarsening of both the grain and dispersoid by annealing of the 0 pct B alloy. The Al_2O_3 dispersoid grows by a factor of 10 during annealing. The grain size also shows about an order-of-magnitude increase. The grain growth observed in the binary alloy, even in the presence of a dispersoid, is not surprising, since the dispersoid particles are coarse and their volume fraction is low. On the other hand, the grain size of the B containing alloy increases by a factor of 2 during

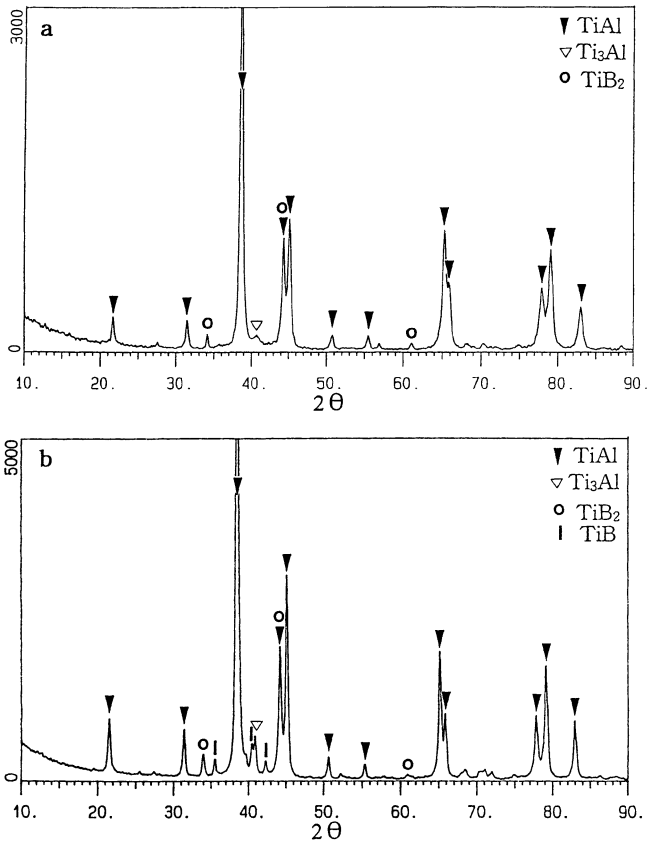

Fig. 6—XRD patterns of 5 pct B alloy after VHPing: (*a*) melt-extracted alloy and (*b*) mechanically milled alloy.

Table II. Variation of O and N Contents and Type of Ti Boride of 5 Pct B Alloy with Processing Step

	O (Wt Pct)	N (Wt Pct)	Observed Boride
As-cast	0.031	0.0009	TiB_2
As-melt extracted	0.077	0.0047	TiB_2
AS-VHPed (non-MMed)*	0.077	0.0026	TiB_2
Annealed (AC,non-MMed)	0.079	0.0023	TiB_2
Annealed (FC, non-MMed)	0.080	0.0025	TiB_2
As-VHPed (MMed)	0.46	0.17	TiB_2, TiB
Annealed (AC, MMed)	0.46	0.13	TiB_2, TiB
Annealed (FC, MMed)	0.45	0.14	TiB_2, TiB

*MMed: mechanically milled.

Table III. Relative Intensities of α_2 and γ Phases ($I_{(201)\alpha 2}/I_{(111)\gamma}$)

	0 Pct B	0.5 Pct B	2 Pct B	5 Pct B
As-VHPed	0.08	0.08	0.07	0.06
Annealed (AC)	0.36	0.26	0.26	0.19
Annealed (FC)	0.18	0.16	0.14	0.07

annealing, which indicates the effectiveness of TiB_2 and TiB in restricting grain growth (Figure 4).

B. *Mechanical Properties*

As shown in Table IV, the as-VHPed specimens exhibit very high compressive yield strength, but show limited ductility. The compression test on the annealed and air-cooled specimens (Figure 7 and 8) reveals that the mechanically milled alloys have considerably higher yield strength than the melt-extracted alloys at all test temperatures. It is believed that the dispersion of Ti_2AlN and Al_2O_3 particles along with refined grain structure is responsible for the high strength of mechanically milled alloys. It also shows that the strength increases with B content for both the melt-extracted alloys and mechanically milled alloys. It has been attempted to quantitavely analyze the contribution of various strengthening mechanisms for the 5 pct B alloy as compared to the 0 pct B alloy. The contribution of the grain boundary strengthening is calculated to be about 627 MPa using $\sigma_0 = 140$ MPa and $K_y = 0.88$ MPa$\sqrt{m}$ obtained for the Ti-48Al-2Cr alloy,[19] which has similar composition and microstructure to the present alloys. The dispersion strengthening effect is calculated as $\Delta\sigma = 253$ MPa by using $\Delta\sigma = (0.13\ G\mathbf{b}/\lambda)\ ln\ (r/\mathbf{b})$, which shows the strength increment due to the unsheared dispersoids.[30] The shear modulus G is 170 GPa,[5] the dislocation Burgers vector **b** is 0.283 nm for the major mobile dislocation 1/2 <110], the particle spacing λ is 88 nm, and the radius of particles r is 10 nm. However, the strength increment due to the dispersion strengthening is overestimated, since λ obtained from the TEM bright-field image is found to be smaller than the actual distance. Nevertheless, the preceding two

Table IV. Compressive Properties of As-VHPed Mechanically Milled TiAl Alloys at Room Temperature

	0 Pct B	0.5 Pct B	2 Pct B	5 Pct B
Yield strength (MPa)	2313.1	2159.8	2407.4	2129.2
Strain to fracture (pct)	7.3	3.0	4.3	6.6

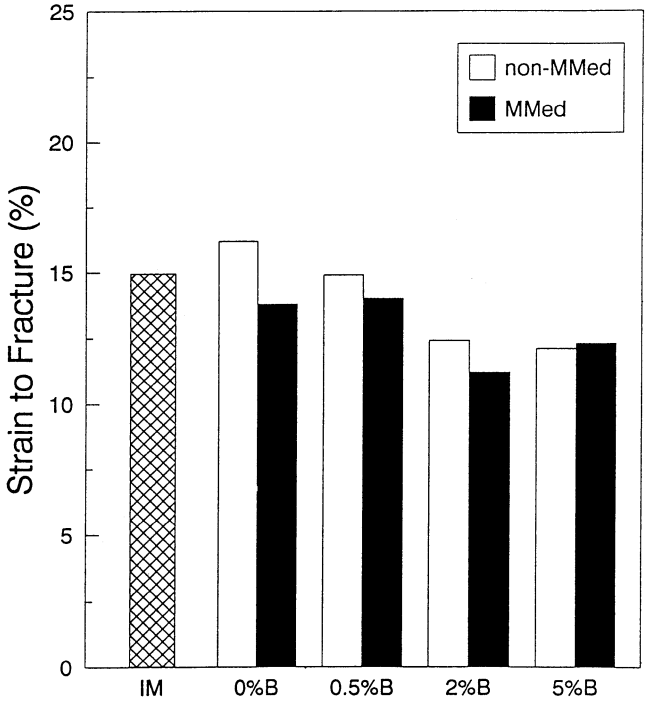

Fig. 7—Strain to fracture at room temperature (MMed: mechanical milling + VHPing + annealing at 1300 °C + air cooling, and non-MMed: melt extraction + VHPing + annealing at 1300 °C + air cooling).

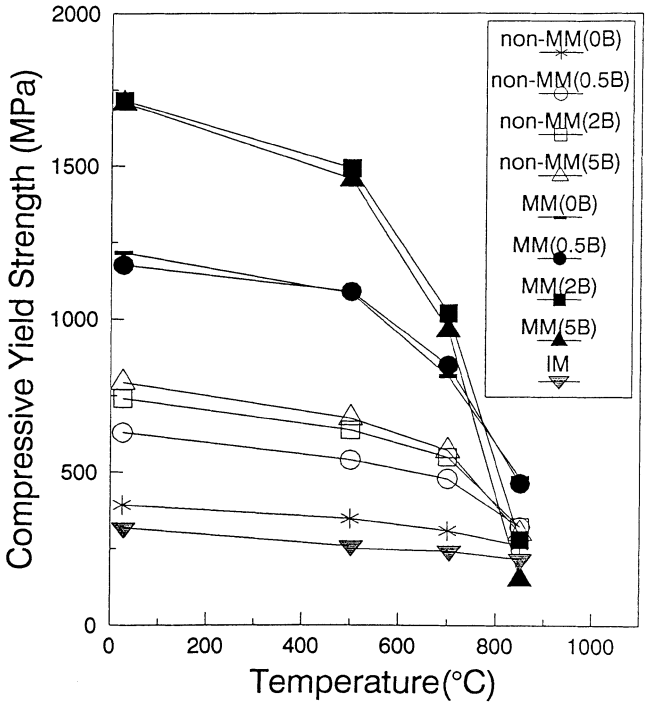

Fig. 8—Temperature dependence of compressive yield strength (MMed: mechanical milling + VHPing + annealing at 1300 °C + air cooling, and non-MMed: melt extraction + VHPing + annealing at 1300 °C + air cooling).

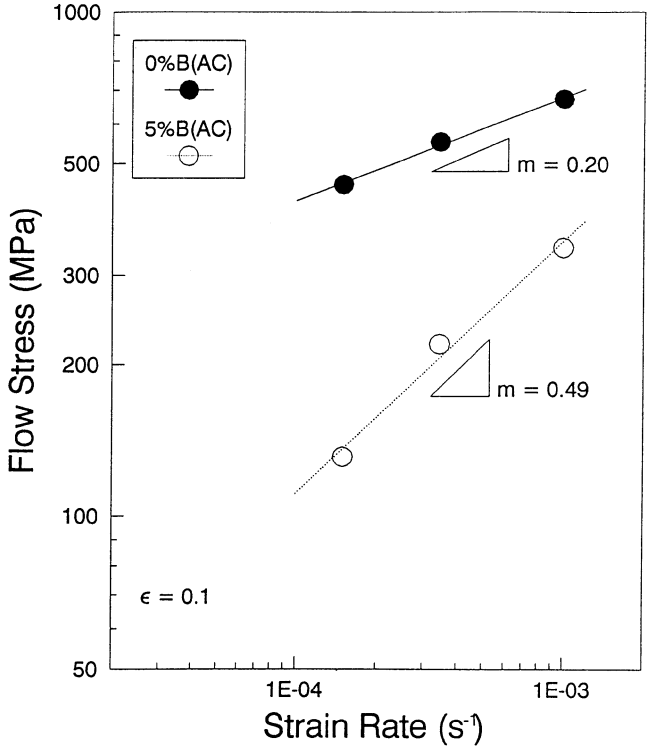

Fig. 9—Stress/strain rate dependence of mechanically milled 0 pct B and 5 pct B alloys at 850 °C (VHPed and annealed at 1300 °C for 5 h, followed by air cooling).

mechanisms can sufficiently explain the observed difference in strength between 5 pct B and 0 pct B alloys. The difference in the amounts of O and N in solid solution and the volume fraction of α_2 phase may also be responsible for the difference in the strength between 5 pct B and 0 pct B alloys. It should be noted here that the contribution of grain refinement is much larger than that of dispersoids, indicating the important role of B in retarding grain growth.

The present alloys show that the yield strength decreases as the temperature increases. This is consistent with the other research results reporting that the inverse relationship of strength to temperature does not exist in multiphase TiAl alloys with fine grains.[31,32] At the test temperature of 850 °C, the 5 pct B alloy with the finest grain shows the lowest yield strength, while the 0 pct B alloy with the coarsest grain shows the highest yield strength. All alloys show that the steady-state deformation with no fracture occurred during the compression test ($\varepsilon > 60$ pct). This implies that there is a change in the deformation mechanism as temperature increases. Comparing the variation of strength with temperature for two structures with different grain sizes, the temperature at which the strengthening effect of B is reversed can be interpreted as the one at which the deformation due to grain boundary sliding becomes dominant.[33] The grain boundary sliding occurs at lower temperatures as the grains become finer, more equiaxed in their morphology, and have higher misorientation angle at the boundary.[34] According to Imayev *et al.*,[35] who observed the high-temperature deformation behavior of the TiAl alloy with very fine grains, the superplastic characteristic (grain boundary sliding) arises at around 900°C, together with visible reduction in flow stress when the grain size is reduced from 2 to 0.2 μm. The strain rate sensitivity indicator, m, was calculated by measuring the change in flow stress with strain rates, in order to find the high-temperature deformation behavior of the 5 pct B alloy with the finest microstructure. As shown in Figure 9, the m values for 5 pct B and 0 pct B alloys are 0.49 and 0.20, respectively. Backofen *et al.*[36] suggested the m value of over 0.3 as an indicator for the superplastic behavior of materials. According to the theories on high-temperature deformation,[33,37,38] when $m \cong 0.2$, the dislocation interactions within the matrix become the rate controlling deformation mechanism, and when $m \cong 0.5$, superplasticity is expected since the deformation is controlled by the grain boundary sliding accommodated by slip. Figure 10 exhibits the structures of 0 pct B and 5 pct B alloys deformed at the strain rate of 3.45×10^{-4} to a strain of 0.1 at room temperature and at 850 °C, respectively. Comparing the deformed structures at room temperature and 850 °C, it is found that coarsenings of grains and dispersoids due to deformation are not observed at 850 °C, and that the deformation is dominated by γ phase deformation with little sign of deformation in α_2 and Ti_2AlN phases, which act as strengthening phases.

In 0 pct B and 5 pct B alloys deformed at room temperature (Figures 10(a) and (c), respectively) and the 0 pct B alloy deformed at 850 °C (Figure 10(b)), the dislocation density is very high with a large amount of deformation twins, whereas in the 5 pct B alloy deformed at 850 °C (Figure 10(d)), the dislocation density is very low with virtually no deformation twins. Figure 11(a) is the deformed structure of the twinned γ region of the 0 pct B alloy deformed at room temperature. In order to identify the major mobile dislocation, $g \cdot \mathbf{b}$ analysis was conducted. It shows that most dislocations are visible with the operating g_{002}, but are invisible with g_{111}, indicating that the major mobile

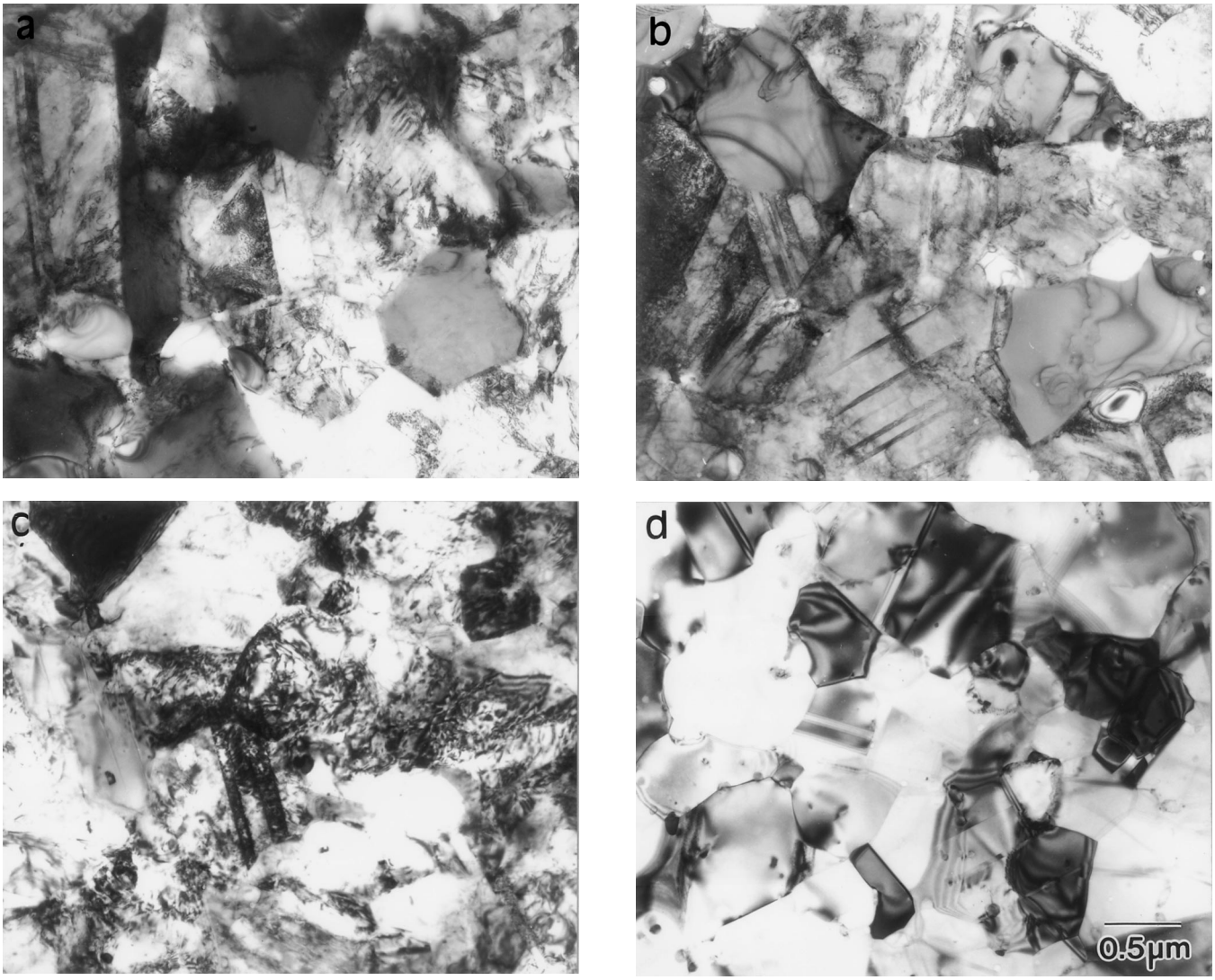

Fig. 10—Bright-field TEM micrographs of deformed specimen: (*a*) 0 pct B alloy deformed at room temperature, (*b*) 0 pct B alloy deformed at 850 °C, (*c*) 5 pct B alloy deformed at room temperature, and (*d*) 5 pct B alloy deformed at 850 °C. All alloys are VHPed and annealed at 1300 °C for 5 h, followed by air cooling.

dislocation is the typical dislocation of 1/2<110] type. Figure 11(b) is the deformed structure of equiaxed γ grain of the 0 pct B alloy deformed at room temperature. The dislocations visible with g_{200} become invisible with g_{002}. These dislocations are also visible with g_{111}, indicating that they are also 1/2 <110] type. The deformed structure of the 0 pct B alloy deformed at 850 °C is shown in Figure 12. The $g\cdot\mathbf{b}$ analysis shows that the dislocations visible with g_{200} become invisible with g_{002}, indicating that they are also 1/2 < 110] type. As shown in Figure 12(b), deformation is mainly concentrated in γ phase. The structure of the 0 pct B alloy deformed at 850 °C differs from that deformed at room temperature in that deformation twins are observed in almost all γ grains of the former. It can also be seen that there is a formation of deformation bands in some of the α_2 particles at 850 °C, while there is no sign of deformation in the α_2 particles at room temperature. The Ti_2AlN phase does not show any sign of deformation at either room temperature or 850 °C. From these observations, it is found that α_2 and Ti_2AlN phases are the strengthening phases acting as obstacles against the deformation. Figure 13(a) shows the deformed structure of the 5 pct B alloy at room temperature. The $g\cdot\mathbf{b}$ analysis shows that major dislocations are again 1/2 <110] type. These dislocations are either tangled around the boride particles (Figure 13(b)) or form Orowan loops (Figure 13(c)). Figure 13(d) is the deformed structure of the 5 pct B alloy at 850 °C. The $g\cdot\mathbf{b}$ analysis again shows that major dislocations are 1/2 <110] type. The 5 pct B alloy deformed at 850 °C can be characterized by the absence of tangled dislocations around the boride particles and Orowan loops, which is different from the 5 pct B alloy deformed at room temperature. It has a very low dislocation density and independently moving dislocations, thus the interaction between dislocations and particles becomes rare at 850 °C. Deformation twins were rarely observed. From these observations, it can be found that the low yield strength of the 5 pct B alloy at 850 °C is attributed to the deformation dominated by grain boundary sliding due to the fine equiaxed grain microstructure with high-angle grain boundaries, as can be seen in its deformation characteristics and m value of 0.49.

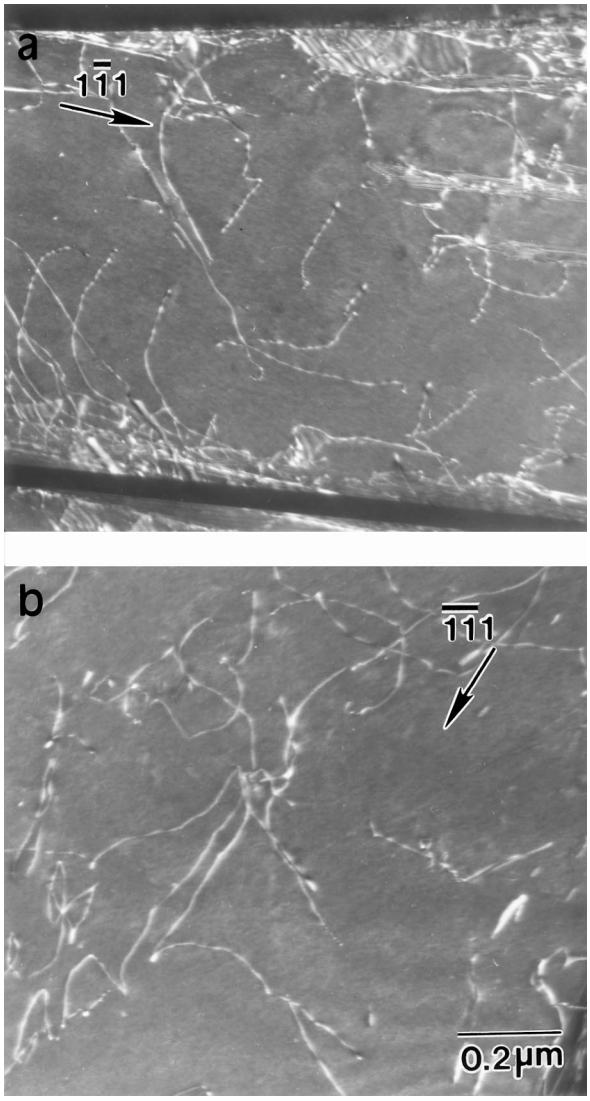

Fig. 11—(*a*) and (*b*) Weak beam images of mechanically milled 0 pct B alloy deformed at 850 °C (VHPed and annealed at 1300 °C for 5 h, followed by air cooling).

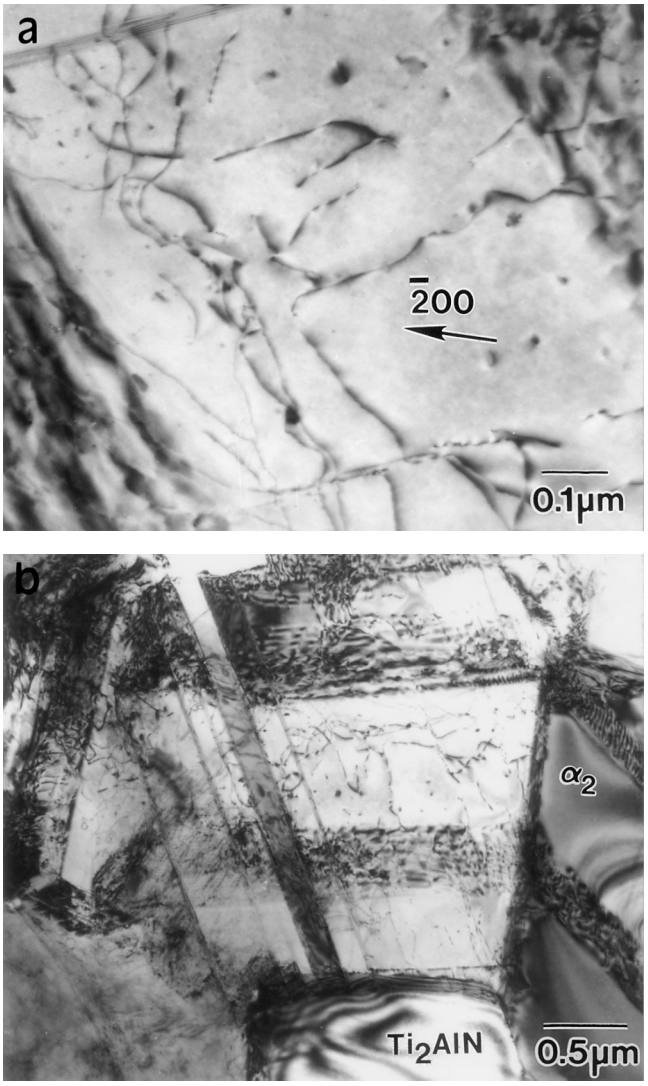

Fig. 12—(*a*) and (*b*) Deformed microstructure of mechanically milled 0 pct B alloy deformed at 850 °C (VHPed and annealed at 1300 °C for 5 h, followed by air cooling).

Figure 14 compares the yield strength values of the air-cooled and furnace-cooled specimens, showing that the former has higher strength than the latter. The grain size and distribution of dispersoids of these two alloys are similar to each other, but the α_2 volume fraction of the air-cooled specimen is higher than that of the furnace-cooled specimen (Table III). The α_2-Ti_3Al has higher strength than γ-TiAl, both at room temperature and 900 °C.[39–42] As was seen in the deformed structure of Figure 8, α_2 phase resists plastic deformation. Therefore, the higher yield strength of the air-cooled specimen over the entire temperature range than that of the furnace-cooled specimen is probably due to the higher volume fraction of α_2 phase in the former.

IV. CONCLUSIONS

In the present study, the effect of B on the microstructure and mechanical properties of mechanically milled TiAl alloys has been investigated.

1. It has been shown that the addition of B has no significant effect on the grain size of mechanically milled alloys consolidated by VHPing at 1000 °C. However, B containing alloys show much smaller grain size than the 0 pct B alloy after annealing at 1300 °C. The grain size of annealed alloys becomes finer as the B content increases. It has been shown that the effect of Ti_2AlN and Al_2O_3 particles on retarding grain growth is much smaller than that of boride particles.
2. Comparison of mechanically milled alloys with melt-extracted alloys after annealing at 1300 °C shows that the former have higher strength with equivalent ductility than the latter, indicating that the beneficial effect of mechanical milling can be retained after high-temperature exposure. Such a beneficial effect can be magnified by the addition of B, showing that the strength increases with B content with no appreciable change in ductility. Up to 700 °C, B containing alloys show higher strength than the 0 pct B alloy due to the strengthening effect of grain refinement and the boride particles in the former. At 850 °C, however, grain boundary sliding becomes

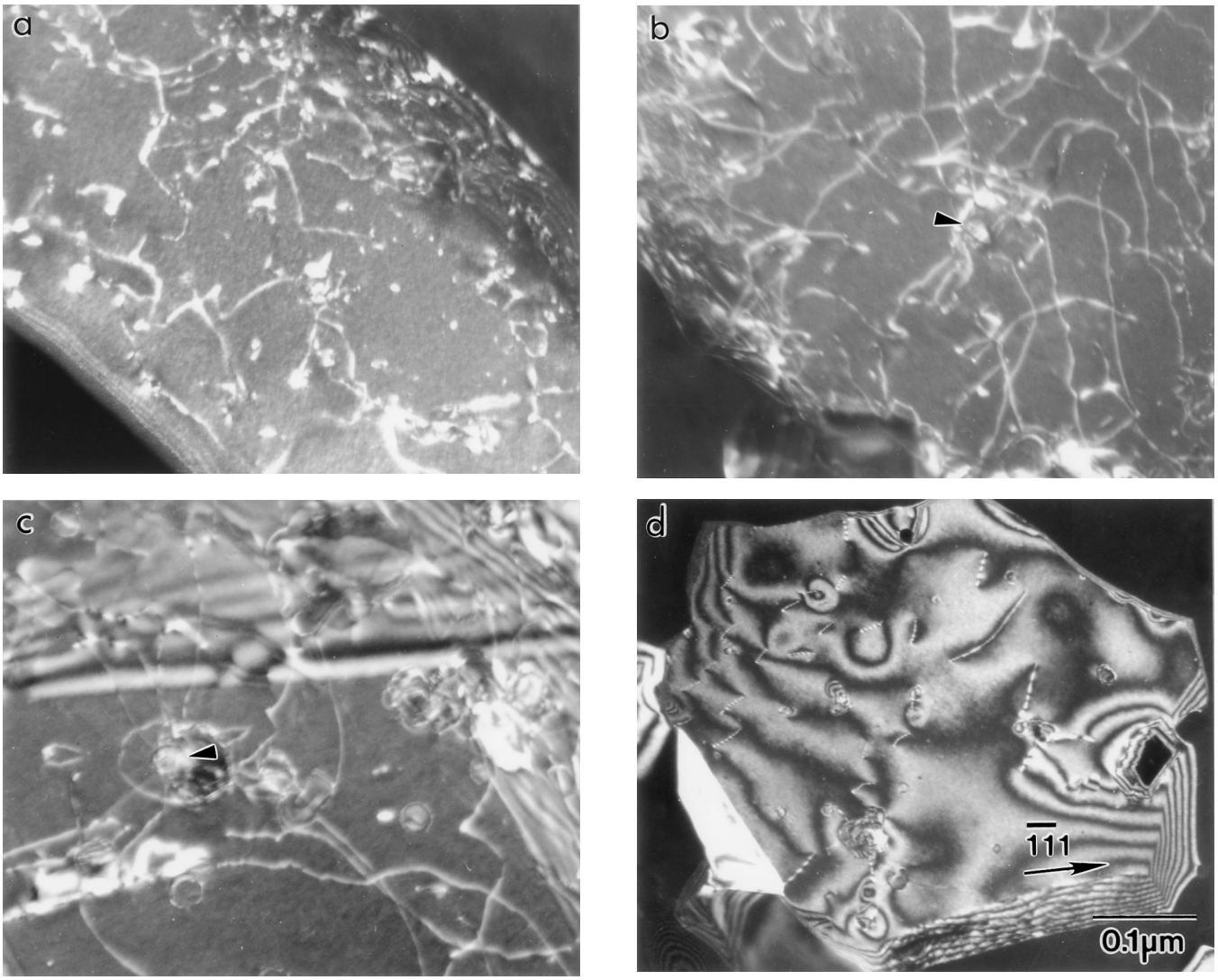

Fig. 13—Weak beam images of mechanically milled 5 pct B alloy (VHPed and annealed at 1300 °C for 5 h, followed by air cooling): (*a*) through (*c*) deformed at room temperature and (*d*) deformed at 850 °C.

dominant for the 5 pct B alloy with the finest grains, resulting in a lower strength than the 0 pct B alloy.

ACKNOWLEDGMENT

This work was supported by the Nano-Structure Technology Project.

REFERENCES

1. H.A. Lipsitt, D. Shechtman, and R.E. Schafrik: *Metall. Trans. A*, 1975, vol. 6A, pp. 1991-96.
2. Y.-W. Kim: *JOM*, 1989, vol. 41, pp. 24-30.
3. M. Yamaguchi and Y. Umakoshi: *Progr. Mater. Sci.*, 1990, vol. 34, p. 1.
4. M. Yamaguchi and H. Inui: *Structural Intermetallics*, TMS Symp. Proc., R. Darolia, J.J. Lewandowski, C.T. Liu, PL. Martin, D.B. Miracle, and M.V. Nathal, eds., TMS, Warrendale, PA, 1993, p. 127.
5. Y.-W. Kim: *JOM*, 1994, vol. 46, pp. 30-40.
6. F.H. Froes, C. Suryanarayana, and D. Eliezer: *J. Mater. Sci.*, 1992, vol. 27, pp. 5113-40.
7. F.H. Froes, C.-G. Li, P.R. Taylor, D. Chellman, F. Hehmann, and C.M. Ward-Close: *Mater. Trans., JIM*, 1996, vol. 37, pp. 389-93.
8. C. Suryanarayana and F.H. Froes: in *Heat-Resistant Materials*, ASM Symp. Proc., K. Natesan and D.J. Tillack, eds., ASM, Materials Park, OH, 1991, pp. 25-34.
9. S.G. Pyo, P. Nash, and N.J. Kim: *Scripta Metall.*, 1996, vol. 34, pp. 1231-35.
10. S.C. Huang and E.L. Hall: *High-Temperature Ordered Intermetallic Alloys IV*, Materials Research Society Symposia Proceedings, L.A. Johnson, D.P. Pope, and J.O. Stiegler, eds., Materials Research Society, Pittsburgh, PA, 1991, vol. 213, p. 827.
11. M. Saqib, I. Weiss, G.M. Mehrotra, E. Clevenger, A.G. Jackson, and H.A. Lipsitt: *Metall. Trans. A*, 1991, vol. 22A, pp. 1721-28.
12. L. Christodoulov, P. Parrish, and C.R. Crowe: *High Temperature/High Performance Composites*, Materials Research Society Symposia Proceedings, F.D. Lemkey, A.G. Evans, S.G. Fishman, and J.R. Strite, eds., Materials Research Society, Pittsburgh, PA, 1989, vol. 120, pp. 29-34.
13. A. Szaruga, L. Rothenflue, R. Srinivasan, and H.A. Lipsitt: *Scripta Metall.*, 1992, vol. 26, pp. 1565-70.
14. H.H. Chung, S.J. Hwang, and N.J. Kim: *Int. J. Non-Equil. Processing*, 1997, vol. 9, pp. 31-40.
15. S.C. Huang and D.S. Shih: *Microstructure/Property Relationship in Titanium Alloys and Intermetallics*, TMS Symp. Proc., Y.W. Kim and R.R. Boyer, eds., TMS, Warrendale, PA, 1991, p. 105.
16. S.G. Pyo, Y.W. Chang, and N.J. Kim: *Met. Mater.*, 1995, vol. 1, pp. 107-15.
17. C. McCullough, J.J. Valencia, C.G. Levi, and R. Mehrabian: *Acta Metall. Mater.*, 1989, vol. 37, pp. 1321-36.

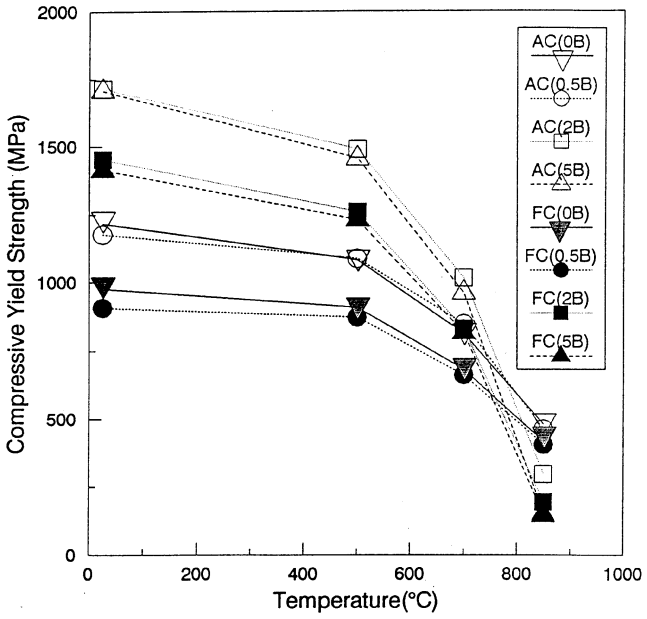

Fig. 14—Effect of cooling rate on the compressive yield strength of various mechanically milled TiAl alloys (VHPed and annealed at 1300 °C for 5 h). FC: furnace-cooled, and AC: air-cooled.

18. Y.W. Kim: in *High-Temperature Ordered Intermetallic Alloys IV*, Materials Research Society Symposia Proceedings, L.A. Johnson, D.P. Pope, and J.O. Stiegler, eds., Materials Research Society, Pittsburgh, PA, 1991, vol. 213, p. 777.
19. C. Koeppe, A. Bartels, J. Seeger, and H. Mecking: *Metall. Trans. A*, 1993, vol. 24A, pp. 1795-1806.
20. C.M. Lombard, R.M. Nekkanti, and V. Seetharaman: *Scripta Metall.*, 1992, vol. 26, pp. 1559-64.
21. S.G. Pyo, H.H. Chung, J.S. Hwang, and Nack J. Kim: *J. Kor. Powder Metall. Inst.*, 1988, vol. 5, pp. 98-110.
22. K.Y. Wang: *J. Mater. Sci.*, 1995, vol. 30, pp 5427-32.
23. H. Mabuchi, H. Tsuda, Y. Nakayama, and E. Sukedai: *J. Mater. Res.*, 1992, vol. 7, p. 894.
24. D.S. Schwartz, P. Fraundorf, and S.M.L. Sastry: *Ultramicroscopy*, 1991, vol. 37, pp. 310-17.
25. M.E. Hyman, C McCullough, J.J. Valencia, C.G. Levi, and R. Mehrabian: *Metall. Trans. A*, 1989, vol. 20A, pp. 1847-59.
26. M.E. Hyman C. McCullough, J.J. Valencia, C.G. Levi, and R. Mehrabian: *Metall. Trans. A*, 1991, vol. 22A, pp. 1647-62.
27. J.J. Valencia, J.P.A. Lofvander, C. McCullough, and C.G. Levi: *Mater. Sci. Eng. A*, 1991, vol. 144A, pp. 25-36.
28. W.E. Frazier and M.J. Kozak: in *High Strength Powder Metallugy Aluminum Alloys II*, G.H. Hildeman and M.J. Kozak, eds., TMS, Warrendale, PA, 1988, p. 103.
29. Y. Yamabe, M. Takeyama, and M. Kikuchi: in *Gamma Titanium Aluminides*, Y.-W. Kim, R. Wagner, and M. Yamaguchi, eds., TMS, Warrendale, PA, 1995, p. 111.
30. G.E. Dieter: *Mechanical Metallurgy*, 3rd ed., McGraw-Hill Book Co., New York, NY, 1986, pp. 212-19.
31. S.C. Huang: *Scripta Metall.*, 1988, vol. 22, pp. 1885-88.
32. T.P. Weihs, V. Zinoviev, D.V. Viens, and E.M. Schulson: *Acta Metall.*, 1987, vol. 35, pp. 1109-18.
33. J.W. Edington, K.N. Melton, and C.P. Cutler: *Progr. Mater. Sci.*, 1976, vol. 21, p. 61.
34. O.D. Sherby and J. Wadsworth: *Progr. Mater. Sci.*, 1989, vol. 33, p. 169.
35. R. Imayev, M. Shagiev, G Salishchev, V. Imayev, and V. Valitov: *Scripta Metall.*, 1996, vol. 34, p. 985.
36. W.A. Backofen, I.R. Turner, and D.H. Avery: *Trans. Am. Soc. Mater.*, 1964, vol. 57, p. 980.
37. O.D. Sherby and P.M. Burke: *Progr. Mater. Sci.*, 1967, vol. 13, p. 325.
38. A. Arieli and A.K. Mukherjee: *Metall. Trans. A*, 1982, vol. 13A, pp. 717-32.
39. T. Kawabata, T. Tamura, and O. Izumi: in *High-Temperature Ordered Intermetallic Alloys III*, C.T. Liu, A.I. Taub, N.S. Stoloff, and C.C. Koch, eds., MRS, Pittsburgh, PA, 1989, vol. 133, p. 329.
40. S.C. Huang and E.L. Hall: *Metall. Trans. A*, 1991, vol. 22A, pp. 427-39.
41. T. Tsuzuku and H. Sato: *J. Phys. IV*, 1993, vol. 3, p. 389.
42. K. Ameyama, A. Miyazaki, and M. Tokizane: in *Superplasticity in Advanced Materials*, S. Hori, M. Tokizane, and N. Furushiro, eds., Japan Society for Research on Superplasticity, Tokyo, Japan, 1991, p. 317.